Novel Model-Based Control Mixing Strategy for a Coaxial Push-Pull Multirotor

Jawhar Chebbi, François Defaÿ, Yves Brière, and Alban Deruaz-Pepin

***Abstract*—A Coaxial push-pull multirotor is a Vertical Take-Off and Landing (VTOL) Unmanned Aerial Vehicle (UAV) having $2n$ ($n \in \mathbb{N}^*$) rotors arranged in n blocks of two coaxial contra-rotating rotors. A model-based control allocation algorithm (mixer) for this architecture is proposed. The novelty of the approach lies in the fact that the coaxial aerodynamic interference occurring between the pairs of superimposed rotors is not neglected but rather nonlinear empiric models of the coaxial aerodynamic thrust and torque are used to build the mixer. Real flight experiments were conducted and the new approach showed promising results.**

***Index Terms*—Aerial systems, mechanics and control, calibration and identification, force control.**

I. Introduction

UNDERACTUATED multirotors are the most widely used Vertical Take-Off and Landing (VTOL) Unmanned Aerial Vehicles (UAV) both for research and industrial applications due to their easy integration and high versatility. The quadcopter is the precursor of these UAVs and remains the most popular one. However, in order to meet increasing safety and payload requirements, new multirotor configurations with more than four motors have been tested and used over the recent years (like hexarotors [1], [2] and octorotors [3]–[5]). One interesting property of underactuated multirotors is that regardless of the number and disposition of the motors, they can be controlled in the same way, using four control inputs corresponding to the total thrust force and to three torques around the three body axes, as long as these control efforts are dispatched to the motors according to the rotors configuration. The algorithm in charge of this allocation is commonly called mixer.

The present paper introduces a model-based mixing strategy applied to a push-pull octorotor, also called X8. The number of rotors is not important for this study, the same approach could be used for any push-pull multirotor. Designing an adapted mixer for this kind of configuration is more challenging than for a normal plane one, if the aerodynamic interaction between each pair of coaxial rotors is taken into account. The relevance of the proposed mixer is discussed by comparing the flight performances to the case of a conventional model-based mixer assuming isolated rotors.

The main contributions of the present paper are first the incorporation of a knowledge about the interference between the rotors' airflows into the control allocation problem, and secondly the use of a nonlinear coaxial rotor torque model to solve the mixing problem instead of a simplified torque to thrust model. In the sequel, the key steps taken to implement the algorithm are presented, from the acquisition of experimental data to simulation and real flight tests. The approach is tested on a coaxial octorotor.

This work was supported by the company Donecle (https://www.donecle.com/) and the lab ISAE-SUPAERO (https://www.isae-supaero.fr/en/research/isae-supaero-research/). This letter was recommended for publication by Associate Editor V. Lippiello and Editor J. Roberts upon evaluation of the reviewers' comments. *(Corresponding author: Jawhar Chebbi.)*

J. Chebbi is with Donecle, Labege, France, and also with Aerospace Vehicles Design and Control Department (DCAS), ISAE-SUPAERO, Toulouse University, Toulouse, France (e-mail: jawhar.chebbi@isae-supaero.fr).

F. Defaÿ is with the Electrical Engineering and Industrial Computer Science Department (GEII), IUT Tarbes, France (e-mail: francois.defay@iut-tarbes.fr).

Y. Brière is with the Aerospace Vehicles Design and Control Department (DCAS), ISAE-SUPAERO, Toulouse University, Toulouse, France (e-mail: yves.briere@isae-supaero.fr).

A. Deruaz-Pepin is with Donecle, Labege, France (e-mail: alban.deruaz-pepin@donecle.com).

Digital Object Identifier 10.1109/LRA.2019.2963652

II. Overview of the Mixing Strategy

The idea behind mixing is to make the resultant torques and force applied by the rotors on the UAV body as close as possible to the requested control signals. To do so, it is essential to know the motors input/output behaviour, hence the name given to this approach: model-based.

The following symbols and notations are used:

- $\boldsymbol{u}^* \in \mathbb{R}^4$ is the vector of control signals computed by the UAV controller: the desired roll, pitch yaw torques (respectively τ_p^*, τ_q^* and τ_r^*) and the total thrust T^* to be applied on the UAV body.
- $\boldsymbol{f}^*$ and $\boldsymbol{Q}^* \in \mathbb{R}^n$ are the vectors of the desired thrust forces and torques on the n coaxial pairs of rotors.
- $\boldsymbol{\delta} \in \mathbb{R}^{2n}$ is the vector of the throttle signals sent to the motors speed controllers, so $\forall i \in \{1..2n\}, 0 \leqslant \delta_i \leqslant 1$.
- $\boldsymbol{f}$ and $\boldsymbol{Q} \in \mathbb{R}^n$ are the vectors of the actual (unknown) thrust forces and torques produced by the n coaxial pairs of rotors.
- $\boldsymbol{u} \in \mathbb{R}^4$ is the vector of the actual (unknown) resultant torques and thrust force applied on the UAV body by the motors.
- $\boldsymbol{P}$ is a virtual function describing the transformation, by the motors, of the throttle commands to thrust forces, $\tilde{\boldsymbol{P}}$ is a model of this function (see IV-A1) and $\tilde{\boldsymbol{P}}^{\dagger}$ is its pseudo-inverse.
- $\boldsymbol{M}$ is a virtual function describing the transformation of the thrust forces to resultant torques and force on the UAV

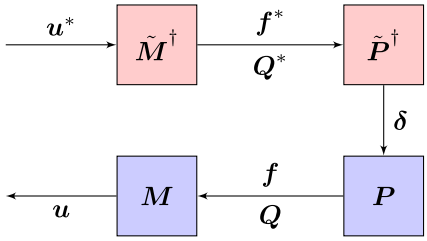

Fig. 1. Block diagram of the data flow from the control outputs $\boldsymbol{u}^*$ to the actual efforts applied on the UAV body $\boldsymbol{u}$.

body, $\tilde{\boldsymbol{M}}$ (see IV-A2) is a model of this function and $\tilde{\boldsymbol{M}}^\dagger$ is its pseudo-inverse.

The different signals introduced above are sequentially related as shown in Fig. 1.

Using this notation, the mixing algorithm goal is to achieve $\boldsymbol{u} = \boldsymbol{u}^*$. Having $\boldsymbol{u} = \boldsymbol{M}(\boldsymbol{P}(\tilde{\boldsymbol{P}}^\dagger(\tilde{\boldsymbol{M}}^\dagger(\boldsymbol{u}^*))))$, the previous equality constraint means that the composition of the inverse mappings with the real system behaviour functions must be equal to identity.

The model $\tilde{\boldsymbol{P}}$ is identified experimentally and inverted numerically. As for the model $\tilde{\boldsymbol{M}}$, it is deduced from the motors disposition and symmetries and inverted analytically as explained in the next section.

III. Related Work

Most of the literature on control allocation techniques for multirotor UAVs is focused on motor failure recovery and saturation handling and not on the main model inversion problem (see for instance [6]–[9]). This is due to the fact that isolated rotors are assumed in most of the cases, making the model inversion straightforward. However this assumption becomes limiting for some configurations where aerodynamic interference between rotors is quite strong like the coaxial case, as in the case of [10] where the control allocation for the octorotor is performed without taking into account the coaxial interaction which is considered as part of unmodelled dynamics. These are estimated using an extended inverse multi-quadratic radial basis function neural network that needs to be trained offline. There are similarly different control techniques to compensate for unmodelled aerodynamic disturbances like extended state observers or external wrench estimators (see for instance [11]). However, unlike adapting the mixer, these methods will account for a lumped disturbance term containing external efforts and modelling uncertainties along with aerodynamic effects. So they should be more efficient when used with a mixer similar to the one proposed in the present work because by doing so, the effects due to rotors' interference are removed (or at least reduced) in feedforward, making the disturbance estimation and rejection easier.

The coaxial propulsion configuration has several advantages such as: the maximisation of available rotor disk surface while keeping a compact UAV body size, the ability to recover motor failures due to hardware redundancy, the enhanced yaw stability given by the disposition of the coaxial contra-rotating rotors which reduces gyroscopic torques on the UAV body and the minimisation of rotor swirl losses for the same reason. With these assets come some complications, mainly the aerodynamic interaction occurring at each pair of coaxial rotors.

This overlapping effect has been identified and studied by aerodynamicists. Leishman [12] for instance models this effect using the simple momentum theory in a particular case where the separation distance equals to the diameter of the rotor, and concludes that this configuration consumes 28% more power than the isolated case. This power efficiency loss is greater when the separation distance is smaller (which is the case for most multirotor UAVs). More recent experimental studies were also performed as in [13] where the thrust (f_u and f_l) and torque (Q_u and Q_l) produced by each rotor were modelled as second-order polynomials of both rotor speeds which extends the usual 1D quadratic model used for a single isolated rotor. A similar approach was also used in [14] where a static coaxial thrust map was built. However the coaxial effect was only modelled by adding a multiplicative loss coefficient to the sum of the thrusts of both isolated rotors. The same approach was followed for the modelling of a coaxial octorotor in [3]. A different model for a coaxial propulsion unit was used in [15] based on Takagi-Sugeno fuzzy interface and surface fitting. However in all of these studies there is no explicit mention of the control allocation problem and it is not clear whether the coaxial models were used for the mixer or not.

The same issue has also been recently raised by new studies on novel omni-directional UAVs where the disposition of rotors makes their aerodynamics mutually influenceable. In [16] the aerodynamic interference between the propellers of the eight rotor omnicopter was not taken into account for the mixing problem. Rather, thrust and torque decrease coefficients were identified experimentally and applied to the motor speeds to compensate for all of the aerodynamic effects. More recently, the same problem was addressed in a more direct way in [17] where a static actuator inverse model that accounts for the interactions between rotors is used for the mixer. It is built by varying the constant parameters of a physical thrust-to-PWM model initially built for one isolated rotor. In the present work, the same thing is done for a coaxial propulsion unit but using a different approach based on numerical inversion of 2D static maps. The obtained mixer is then compared to a non-coaxial one in order to assess the relevance of considering the overlapping effect.

IV. Application to the X8 Configuration

The used X8 UAV is depicted in Fig. 7(b).

A. Modelling Step

1) Model $\tilde{\boldsymbol{P}}$: The actuators of most modern common multirotors consist of fixed-pitch propellers attached to brushless electrical motors driven by Electronic Speed Controllers (ESC). The ESCs monitor the motors' angular rates based on the percentage of throttle $\boldsymbol{\delta}$ requested by the pilot (human or automatic).

In this study, the considered propulsion unit is a pair of coaxial contra-rotating rotors. This leads to models with two inputs. To identify the models, the coaxial test bench shown in Fig. 2 was used. This test bench allows to control the two

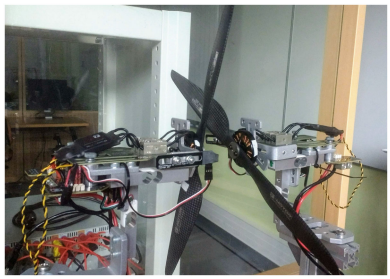

Fig. 2. Coaxial test bench at DCAS (Department of Aerospace Vehicles Design and Control, ISAE-SUPAERO).

motors independently in hovering-like conditions. It consists of two RCBenchmark thrust-stands equipped with optical speed sensors, load cells and electronic boards to connect the ESCs and the USB data acquisition ports. The available measurements include the electrical currents, the propellers angular rates and the generated thrusts and torques. The distance between both stands is adjustable and was set to 6.14 cm as the UAV used for the experiments. The software used to acquire data and to control simultaneously both motors was developed in MATLAB.

The recorded angular rates, thrusts and torques are used to build maps relating any individual output to both PWM inputs. Individual measurements are added up to obtain total coaxial thrust and torque values. It is worth mentioning that the rotor aerodynamics suggest that the thrust and torque models depend directly on the rotor angular rates. But in our case the ESCs are not equipped with speed measurements, so this information is not accessible on-board. Besides, it is established that the conversion of PWM to angular rate by the ESC is close to a linear mapping [18], for a fixed battery voltage. So it makes sense to relate the thrust and torque directly to the PWM values (or equivalently to the throttle inputs). The chosen model structure is inspired from [13] where second-order two-dimensional polynomials are used. The difference is, that in this work, all of the polynomial coefficients were kept as degrees of freedom and not only the homogeneous part, allowing richer models and better data fit. Therefore, the considered total thrust and torque empirical models are as follows

$$f = \begin{bmatrix} \delta_u^2\delta_l^2 & \delta_u^2\delta_l & \delta_u^2 & \delta_u\delta_l^2 & \delta_u\delta_l & \delta_u & \delta_l^2 & \delta_l \end{bmatrix} \begin{bmatrix} a_1 \\ \vdots \\ a_8 \end{bmatrix} \tag{1a}$$

$$Q = \begin{bmatrix} \delta_u^2\delta_l^2 & \delta_u^2\delta_l & \delta_u^2 & \delta_u\delta_l^2 & \delta_u\delta_l & \delta_u & \delta_l^2 & \delta_l \end{bmatrix} \begin{bmatrix} b_1 \\ \vdots \\ b_8 \end{bmatrix} \tag{1b}$$

where the index u refers to the upper motor and the index l to the lower one.

Polynomial equations 1 could be written in the following compact form

$$\boldsymbol{y} = \boldsymbol{A}.\boldsymbol{\theta} \tag{2}$$

where $\boldsymbol{\theta} \in \mathbb{R}^8$ is the vector of parameters to estimate, $\boldsymbol{y} \in \mathbb{R}^N$ ($N \in \mathbb{N}^*$) is the vector of all measured torque or thrust data and $\boldsymbol{A} \in \mathbb{R}^N \times \mathbb{R}^8$ is the regressors matrix. The least-squares solution is chosen, which corresponds to

$$\hat{\boldsymbol{\theta}} = \left(\boldsymbol{A}^T\boldsymbol{A}\right)^{-1}\boldsymbol{A}^T.\boldsymbol{y}. \tag{3}$$

The result of this second order polynomial fit (Table I) is good as seen in Fig. 3.

2) Model $\tilde{\boldsymbol{M}}$: Let the actuation vector $\boldsymbol{u}$ be written as $\boldsymbol{u} = [\tau_p \ \ \tau_q \ \ \tau_r \ \ T]^T$. The thrust and aerodynamic torque produced by the i^{th} coaxial unit of rotors ($i \in \{1, .., 4\}$) are noted f_i and Q_i respectively. The lever arm l is also introduced. One can then write the following equations.

$$\begin{cases} \tau_p = l\left(-f_1 + f_2 + f_3 - f_4\right) \\ \tau_q = l\left(f_1 + f_2 - f_3 - f_4\right) \\ \tau_r = Q_1 - Q_2 + Q_3 - Q_4 \\ T = f_1 + f_2 + f_3 + f_4 \end{cases}. \tag{4}$$

Note that those are the same equations for a quadrotor UAV, which is expected because the four pairs of coaxial rotors are considered as a single unit each.

The difference however, is that in the case of a quadrotor mixer, the torques need to be linked to the thrust in order to be able to invert the problem. But in the octorotor case, there are more degrees of freedom allowing to achieve independently torque and force commands as will be shown in Section IV-B2. This is one of the highlights of the proposed strategy which brings in theory more torque and hence yaw stability and efficiency.

Equation 4 can be written in the following compact linear form

$$\boldsymbol{u} = \tilde{\boldsymbol{M}} \begin{bmatrix} \boldsymbol{f} \\ \boldsymbol{Q} \end{bmatrix}. \tag{5}$$

B. Inverting Step

1) Inversion of $\tilde{\boldsymbol{M}}$: This step could be interpreted as a constrained quadratic programming optimisation problem

$$\begin{cases} \boldsymbol{\eta}^* = \mathbf{arg}\min\left(\boldsymbol{\eta}^T\boldsymbol{\eta}\right) \\ \boldsymbol{u}^* = \tilde{\boldsymbol{M}}\boldsymbol{\eta}^* \end{cases} \tag{6}$$

where $\boldsymbol{\eta} = [\frac{\boldsymbol{f}}{\boldsymbol{Q}}]$ is the effort (force and thrust) vector produced by all four pairs of coaxial rotors.

Note: In reality there are additional inequality constraints related to the motors' saturation limits. But the problem is solved by considering the nominal case and when saturation occurs a "desaturation" routine inspired by the algorithm used in PX4 Pixhawk* Software leads to a reduction in the requested total thrust or torque by the needed amount to prevent saturation. This algorithm was adapted for the presented model-based mixer.

The solution to equation 6 could then be given by the Moore pseudo-inverse, which is commonly used for multirotor mixers

*DOI https://zenodo.org/record/3228694

TABLE I
COAXIAL THRUST AND TORQUE MODELS PARAMETERS

	Polynomial coefs θ				R^2	Residual	Confidence Intervals			
$f(\delta_u, \delta_l)$	5.2075	-2.1892	12.3604	-10.2432	99.6053%	$0.3105N$	$\pm$1.0782	0.9468	0.1623	0.9468
	4.4427	2.7640	12.2092	0.2363			$\pm$0.7925	0.1190	0.1623	0.1190
$Q(\delta_u, \delta_l)$	-0.0673	-0.0606	-0.1312	0.0953	99.83%	$0.0037Nm$	$\pm$0.0129	0.0114	0.0019	0.0114
	0.0364	-0.0907	0.1441	0.0720			$\pm$0.0095	0.0014	0.0019	0.0014

where $n > 4$ (see for instance [7], [19]–[21] and [22]).

$$\boldsymbol{\eta}^* = \tilde{\boldsymbol{M}}^T \left(\tilde{\boldsymbol{M}}\tilde{\boldsymbol{M}}^T\right)^{-1} \boldsymbol{u}^* \tag{7}$$

$$= \tilde{\boldsymbol{M}}^\dagger \boldsymbol{u}^*. \tag{8}$$

2) Inversion of $\tilde{\boldsymbol{P}}$: The final step is to find the throttle input commands corresponding to any desired effort vector $\boldsymbol{\eta}^*$ (corresponding to any desired control vector $\boldsymbol{u}^*$). To do so, the two-dimensional quadratic maps built previously need to be inverted. Note that if the rotors are assumed to be isolated, this inversion taking requested force and torque commands as inputs, is not possible, because for one throttle level, one isolated rotor produces only one possible pair of torque and thrust. That is why in this case, a different torque model is used assuming that for an isolated rotor the steady aerodynamic torque is roughly proportional to the thrust with a constant ratio that depends on blade geometry [12]. With this assumption, the only remaining variable is the thrust and the inversion is then straightforward. In fact, the thrust would be proportional to the squared angular rate [23], so the square root is simply taken and finally the mapping from the angular rate to throttle input is linear.

In the considered coaxial two-dimensional case, no torque-to-thrust proportionality is assumed but the additional degree of freedom is used to find the pair of throttle values that give the requested coaxial thrust and torque. This is the main novelty of the present approach. It is not easy to obtain an analytic solution to this coupled problem, so a numerical one was built using MATLAB.

The idea of the algorithm is to first represent the thrust and torque polynomial models in Fig. 3 as planar colour maps an in Fig. 4. Using this data representation, a desired thrust (torque) value corresponds to an iso-curve on the colour map Fig. 4(a) (Fig. 4(b)). So to any thrust-torque pair correspond two curves of pixels on two images. Two masks are then built by setting the pixels on the iso-curve to 1 and the rest of the image to 0. The intersection point, if it exists, is then the pixel having a value equal to 2 on the mask resulting from the sum of both images. The coordinates of the intersection point is the required PWM pair to achieve the requested thrust and torque. This process is made easier thanks to the matrix computation capabilities of MATLAB.

Inverted thrust and torque to throttle maps of an upper bound precision equal to 0.1 N on the thrust and equal to 9.10^{-4} Nm on the torque were built, they are shown in Fig. 5. These maps show, among other things, that there is a zone of achievable thrust-torque pairs by the coaxial propulsion unit, meaning that the available range of torque varies with the thrust level. This brings a better physical insight to the mixing problem. In order to implement these inverted mappings, they were approximated by high order polynomial interpolation functions of two variables.

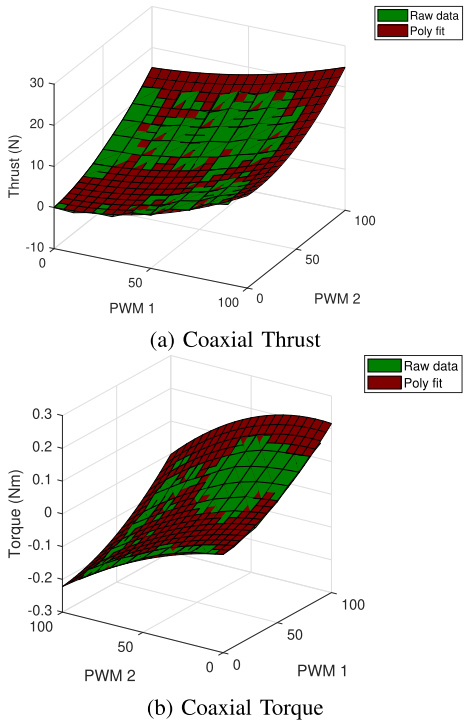

(a) Coaxial Thrust

(b) Coaxial Torque

Fig. 3. Coaxial thrust and torque model maps (red) vs raw data (green).

Note: The voltage effect was also taken into account by multiplying the thrust and torque maps using an experimentally identified voltage correction coefficient that varies with the measured battery voltage on-board.

V. PERFORMANCE COMPARISON WITH A CONVENTIONAL APPROACH

The presented coaxial mixer is compared to a simple one built assuming isolated rotors. The inverted model in this case $\tilde{\boldsymbol{P}}^\dagger$ is a simple 1D quadratic mapping transforming a thrust set-point to its corresponding throttle level. As for $\tilde{\boldsymbol{M}}^\dagger$, it is built after relating each rotor torque to the corresponding thrust: $Q_i = \kappa_t f_i, \forall i \in \{1..8\}$. It should be noted that this torque model not only does not capture the coaxial effect, but is also over-simplistic even for an isolated rotor. In fact, as noted in [24], making κ_t dependent on the thrust gives more accurate results but it leads to an iterative mixer. In the present work, it is possible to easily avoid such iterative solutions while using the full torque nonlinear model by taking advantage of the additional degree of freedom provided by the coaxial configuration.

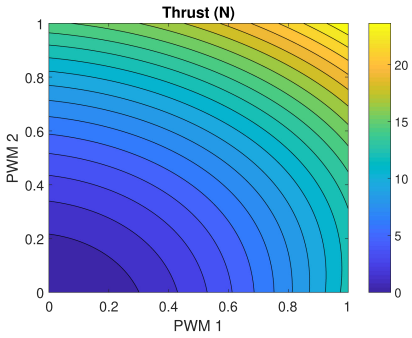

(a) Coaxial Thrust

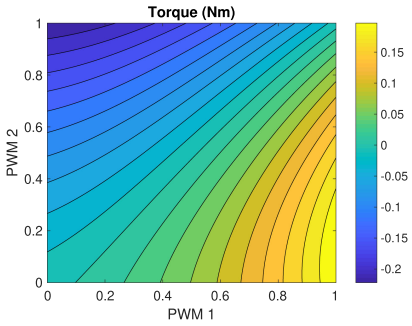

(b) Coaxial Torque

Fig. 4. Coaxial thrust and torque colour maps.

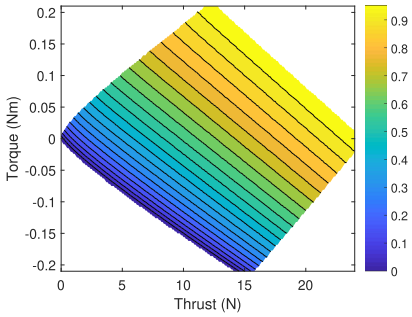

(a) Upper Throttle

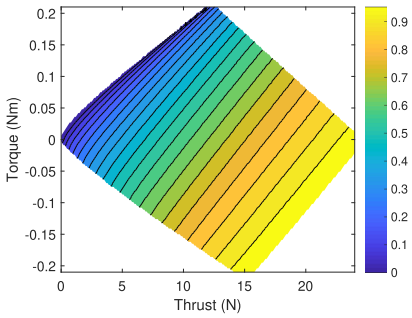

(b) Lower Throttle

Fig. 5. Coaxial inverted model colour maps.

A. Static Simulation Tests

The main advantage of the new coaxial mixer is the way the yaw control is processed. To visualise it, let us consider the case of a thrust command of 40 N (so 10 N per coaxial unit) and several samples of torque commands varying within the maximal available torque range. The (thrust, torque) points in the admissible operating zone are drawn for each of the four coaxial propulsion units in Fig. 6 considering both mixers. It is clear that the coaxial mixer keeps the thrust constant on each propulsion unit while achieving the requested torque, whereas the simple mixer leads to varying thrust levels on the coaxial mixers because the performance degradation of the lower rotor is not taken into account. Another advantage coming from the additional degree of freedom of torque, is that for zero yaw commands, there are in theory no residual torques on the four propulsion units.

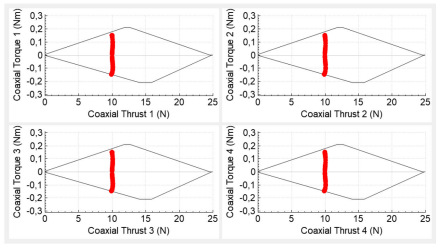

(a) Coaxial Mixer

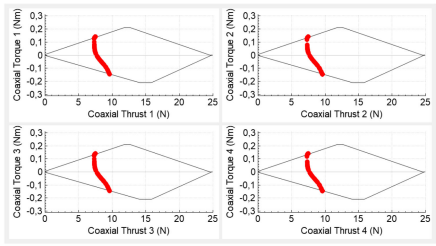

(b) Simple Mixer

Fig. 6. Mixers' handling of yaw commands.

It should be noted that even with the coaxial mixer the single thrust levels on the rotors cannot be kept constant under non zero yaw commands because the speeds of motors need to be changed anyway. However having the four pairs of superimposed rotors produce the same thrust should lead to a smoother yaw behaviour and to less mechanical stress on the multirotor arms. It is like having a quadrotor perform yaw manoeuvres without changing the thrust on the opposed rotors.

B. Real Flight Tests

Real flight tests were performed at the ISAE-SUPAERO robotics room equipped with the motion capture system Optitrack. The UAV is a square-shaped X8 with a diameter equal to 0.9 m, it weighs 3.2 kg and has for principal rotational inertia moments $I_x = 0.0797$ kg.m^2, $I_y = 0.0874$ kg.m^2 and $I_z = 0.1604$ kg.m^2 (see Fig. 7). The UAV controller and mixer were implemented on a Dropix PX4 board. A NVIDIA TX1 board was additionally used to ensure a stable UDP connection with the motion capture system and the ground station software. It communicates with the PX4 board through a serial link. The controller runs at a sampling time of 5 ms and the Optitrack measurement delay is about 50 ms.

The conducted experiment consisted of two hovering flights (one with the simple mixer and the other with the coaxial one)

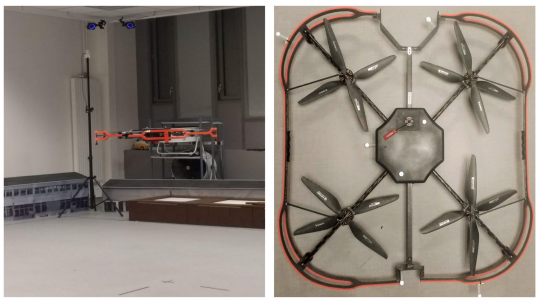

(a) During flight tests (b) Top view

Fig. 7. The coaxial octorotor used for the experiments.

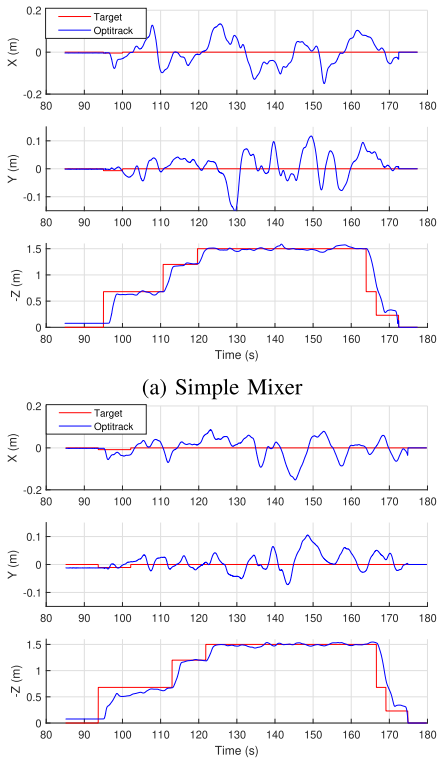

(a) Simple Mixer

(b) Coaxial Mixer

Fig. 8. Position Trajectory Tracking: Reference (Red) vs Measured (Blue).

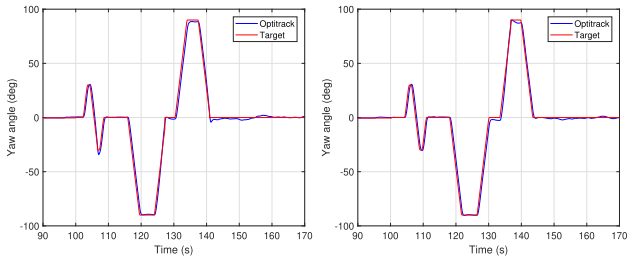

(a) Simple Mixer (b) Coaxial Mixer

Fig. 9. Yaw Profile Tracking: Reference (red) vs Measured (blue).

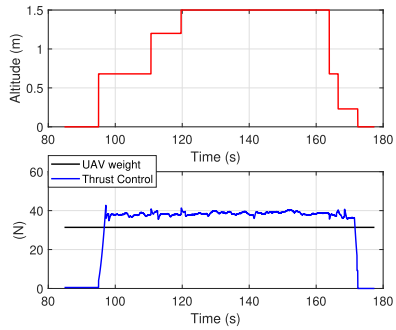

(a) Simple Mixer

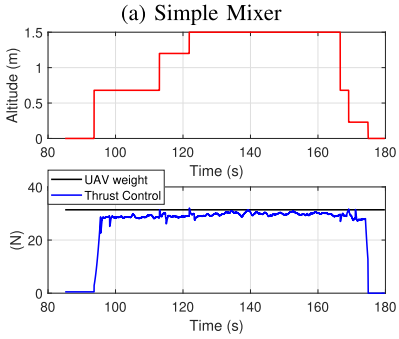

(b) Coaxial Mixer

Fig. 10. Thrust force command (blue) compared to the UAV weight (black) - Upper figures show the corresponding flight altitude phase.

at constant x and y, disturbed with the same manoeuvres on altitude z and yaw, the trajectories are shown in Fig. 8 and Fig. 9. This flight allows to analyse the decoupling performance of the controller in the horizontal plane (x and y axes) while moving along the other degrees of freedom (z and yaw). Baseline position and attitude PID controllers were tuned to guarantee stability and achieve a reasonable trajectory tracking. The sole difference between the two experiments is the mixer algorithm: exactly the same control structure and parameter values were used in both cases in order to be able to isolate the control allocation effect. The results are discussed below.

The main difference between the two mixers is depicted in Fig. 10. The thrust control signal, i.e. the signal sent to the mixer to generate the PWMs based on the inverted rotors model, obtained when the coaxial mixer is used (Fig. 10(b)) is much closer to the hovering equilibrium thrust (the UAV weight). One can see that in contrast, using the simple mixer results in an over-estimation of the needed total thrust (Fig. 10(a)) because the actual equilibrium throttle, reached thanks to the altitude closed loop control, would lead to higher thrust when no coaxial loss is considered. In fact, if the rotors were isolated, the equilibrium would have been achieved for a much lower throttle level because the rotors would be more efficient.

Although the coaxial case leads to a better estimation of the total thrust than the simple mixer, it is still under-estimated as seen in Fig. 10(b). This slowly varying offset of about 2 N cannot be explained by the voltage drop because a compensation is added to adjust the coaxial models when the battery voltage changes. However, it could be due to modelling inaccuracies since those can reach 1.242 N in the worst case (based on thrust residual value in Table I). Additionally, the presence of

TABLE II
POSITION TRACKING (x,y,z): MEAN SQUARED ERROR (MSE), MEAN ABSOLUTE ERROR (MAE) AND MAXIMUM ABSOLUTE ERROR (MaxAE)

	MSE (m^2)			MAE (m)			MaxAE (m)		
Coaxial	$1.6e^{-3}$	$0.7e^{-3}$	$0.5e^{-3}$	0.028	0.020	0.019	0.130	0.078	0.062
Simple	$2.9e^{-3}$	$1.8e^{-3}$	$1.1e^{-3}$	0.039	0.029	0.026	0.144	0.156	0.080

aerodynamic effects induced in the rather small flying area can cause a change of the rotors aerodynamic performance, for instance the ground effect. This effect increases the lift of the rotors [12] and as a result decreases the power needed to be produced by the motors. This could be the reason why the coaxial thrust control gets slightly higher and approaches more the weight of the UAV as it flies higher (Fig. 10(b)).

Furthermore, analysing the position tracking performances in both cases (Fig. 8) shows that using the coaxial mixer leads to a better precision (see Table II, where z is considered during the 1.5 m phase). This means that by adapting the mixer architecture to the UAV, and without any modification of the control parameters, it is possible to reduce the coupling effects between yaw and the other degrees of freedom. The same tendency was verified on other flights.

No significant yaw tracking amelioration was noticed in the coaxial case. This could be due to the fact that the yaw rate was limited in the considered experiments. Yaw control performance could be further investigated by applying more aggressive manoeuvres.

VI. CONCLUSION

A new mixer algorithm adapted to any push-pull multirotor aerial vehicle has been presented. The main highlight of the proposed strategy is that it does not neglect the aerodynamic interaction between the coaxial rotors.

The actuators models identification was described and the obtained models were used in the mixing problem which is defined as a two-step two-dimensional inversion problem. The first inversion step is a well known pseudo-inversion of the control allocation matrix, and the second step is done numerically. This new strategy was successfully tested on a real UAV. It resulted in a better on-line estimation of the total thrust and less coupling between the multirotor axes compared to a conventional model-based mixer.

REFERENCES

[1] S. Pathak, R. Poudel, R. K. Maskey, and P. L. Shrestha, "Design and development of hexa-copter for environmental research," in *Proc. 11th Int. Conf. ASIAN Community Knowl. Netw. Economy, Soc., Culture Environmental Stability*, Kathmandu, Nepal, 2015.

[2] B. Y. Suprapto, M. A. Heryanto, H. Suprijono, J. Muliadi, and B. Kusumoputro, "Design and development of heavy-lift hexacopter for heavy payload," in *Proc. Int. Seminar Appl. Technol. Inf. Commun.: Empowering Technol. Better Human Life, iSemantic*, 2018, vol. 2018, pp. 242–246.

[3] M. Saied, D. AlShamaa, H. Shraim, C. Francis, B. Lussier, and I. Fantoni, "Model identification and validation for translational movements of an octorotor UAV," in *Proc. Workshop Res., Educ. Develop. Unmanned Aerial Syst.*, 2016, pp. 102–108.

[4] S. J. Haddadi and P. Zarafshan, "Design and fabrication of an autonomous Octorotor flying robot," in *Proc. Int. Conf. Robot. Mechatronics*, Tehran, Iran, 2015, pp. 702–707.

[5] V. G. Adîr, A. M. Stoica, and J. F. Whidborne, "Modelling and control of a star-shaped octorotor," *Appl. Mechanics Materials*, vol. 327, pp. 994–998, 2013.

[6] Y. Liu, H. Wang, S. Member, and L. Guo, "Composite robust Hinfty control for uncertain stochastic nonlinear systems with state delay via disturbance observer," *Trans. Autom. Control*, vol. 9286, pp. 1–8, 2018.

[7] A. Marks, J. F. Whidborne, and I. Yamamoto, "Control allocation for fault tolerant control of a VTOL octorotor," in *Proc. UKACC Int. Conf. Control*, Cardiff, UK, 2012, pp. 357–362.

[8] J. C. Monteiro, F. Lizarralde, and L. Hsu, "Optimal control allocation of quadrotor UAVs subject to actuator constraints," in *Proc. Amer. Control Conf.*, 2016, vol. 2016, pp. 500–505.

[9] D. T. Nguyen, D. Saussie, and L. Saydy, "Fault-tolerant control of a hexacopter UAV based on self-scheduled control allocation," in *Proc. Int. Conf. Unmanned Aircr. Syst.*, 2018, pp. 385–393.

[10] R. ul Amin, I. Inayat, and L. Ai Jun, "Finite time position and heading tracking control of coaxial octorotor based on extended inverse multi-quadratic radial basis function network and external disturbance observer," *J. Franklin Inst.*, vol. 356, no. 8, pp. 4240–4269, 2019.

[11] F. Ruggiero, J. Cacace, H. Sadeghian, and V. Lippiello, "Passivity-based control of VToL UAVs with a momentum-based estimator of external wrench and unmodeled dynamics," *Robot. Auton. Syst.*, vol. 72, pp. 139–151, 2015. [Online]. Available: http://dx.doi.org/10.1016/j.robot.2015.05.006

[12] J. G. Leishman, *Principles of Helicopter Aerodynamics*, 2nd ed. Cambridge, U.K.: Cambridge Univ. Press, 2006.

[13] S. Prothin and J.-m. Moschetta, "A vectoring thrust coaxial rotor for micro air vehicle: Modeling, design and analysis," in *Proc. 3AF 48th Int. Symp. Appl. Aerodynamics*, Saint Louis, France, 2013.

[14] A. Koehl, H. Rafaralahy, M. Boutayeb, and B. Martinez, "Aerodynamic modelling and experimental identification of a coaxial-rotor UAV," *J. Intell. Robotic Syst.: Theory Appl.*, vol. 68, no. 1, pp. 53–68, 2012.

[15] P. Gasior, A. Bondyra, S. Gardecki, W. Giernacki, and A. Kasinski, "Thrust estimation by fuzzy modeling of coaxial propulsion unit for multirotor UAVs," in *Proc. IEEE Int. Conf. Multisensor Fusion Integration Intell. Syst.*, 2017, pp. 418–423.

[16] D. Brescianini and R. D'Andrea, "An omni-directional multirotor vehicle," *Mechatronics*, vol. 55, pp. 76–93, 2018.

[17] E. Dyer, S. Sirouspour, and M. Jafarinasab, "Energy optimal control allocation in a redundantly actuated omnidirectional UAV," in *Proc. Int. Conf. Robot. Autom.*, Montreal, Canada, May 2019, pp. 5316–5322. [Online]. Available: https://ieeexplore.ieee.org/document/8793549/

[18] M. Cunningham and J. E. Hubbard, "System identification of a multi-rotor UAV actuator," in *Proc. AIAA Atmospheric Flight Mechanics Conf.*, Texas, 2017. [Online]. Available: http://arc.aiaa.org/doi/10.2514/6.2017-1187

[19] Y. Bouzid, "Guidance and control systems for autonomous aerial vehicles navigation," Ph.D. dissertation, Université Paris Saclay, 2018.

[20] G. P. Falconi, J. Angelov, and F. Holzapfel, "Hexacopter outdoor flight test results using adaptive control allocation subject to an unknown complete loss of one propeller," in *Proc. Conf. Control Fault-Tolerant Syst.*, 2016, vol. 2016, pp. 373–380.

[21] D. Kotarski and M. Engineering, "Mathematical modelling and dynamics analysis of flat multirotor configurations 2 multirotor UAV dynamic model," *WSEAS Trans. Syst.*, vol. 16, pp. 47–52, 2017.

[22] B. Wang and Y. Zhang, "An adaptive fault-tolerant sliding mode control allocation scheme for multirotor helicopter subject to simultaneous actuator faults," *IEEE Trans. Ind. Electron.*, vol. 65, no. 5, pp. 4227–4236, May 2018.

[23] B. Whitehead and S. Bieniawski, "Model reference adaptive Control of a quadrotor UAV," in *Proc. AIAA Guid., Navigation, Control Conf.*, Toronto, Canada, 2010. [Online]. Available: http://arc.aiaa.org/doi/10.2514/6.2010-8148

[24] M. Faessler, D. Falanga, and D. Scaramuzza, "Thrust mixing, saturation, and body-rate control for accurate aggressive quadrotor flight," *IEEE Robot. Autom. Lett.*, vol. 2, no. 2, pp. 476–482, 2017. [Online]. Available: http://ieeexplore.ieee.org/document/7784809/